Monthly Notices
of the
ROYAL ASTRONOMICAL SOCIETY

MNRAS **477,** 5358–5366 (2018)
Advance Access publication 2018 April 14

doi:10.1093/mnras/sty918

Observation of variable pre-eclipse dips and disc winds in the eclipsing LMXB XTE J1710-281

Gayathri Raman,[1]★ Chandreyee Maitra[2,3] and Biswajit Paul[1]★

[1]*Department of Astronomy and Astrophysics, Raman Research Institute, Sadashivanagar, Bangalore 560080, India*
[2]*Laboratoire AIM, IRFU/Service d'Astrophysique - CEA/DSM - CNRS - Universite Paris Diderot, Bat. 709, CEA-Saclay, F-91191 Gif-sur-Yvette Cedex, France*
[3]*Max-Planck-Institut für extraterrestrische Physik, Giessenbachstraße, D-85748 Garching, Germany*

Accepted 2018 April 10. Received 2018 April 10; in original form 2016 October 27

ABSTRACT

We report the first detection of highly ionized Fe species in the X-ray spectrum of the eclipsing and dipping Low-Mass X-ray Binary XTE J1710-281. Using archival *Chandra* and *Suzaku* observations, we have carried out a spectro-timing analysis of the source during three different epochs. We compare the average orbital profile and obtain differences in pre-eclipse dip morphologies between different observation epochs. We observe an orbit-to-orbit evolution of the dips for the first time in this source in both the *Chandra* observations, reflecting changes in the structure of the accretion disc in time-scales of hours. We further perform intensity resolved spectroscopy for both the *Chandra* and the *Suzaku* data to characterize the changes in the spectral parameters from the persistent to the dipping intervals. We find that the absorbers responsible for the dips can be best described using a partially ionized partial covering absorber, with an ionization parameter, log(ξ) of $\sim$2. The photon index of the source remained at $\sim$2 during both the *Chandra* and the *Suzaku* observations. In the 0.6–9 keV *Suzaku* spectra, we detect a broad 0.72 keV Fe L-alpha emission line complex and two narrow absorption lines at $\sim$6.60 and $\sim$7.01 keV. The highly ionized Fe line signatures, being an indicator of accretion disc winds, have been observed for the first time in XTE J1710-281.

Key words: accretion, accretion discs – binaries: eclipsing – stars: neutron – X-rays: binaries.

1 INTRODUCTION

Accreting low-mass X-ray binary (LMXB) systems contain a compact object in a binary configuration with a mass-donating low-mass companion star (Lewin & Clark 1980). A small subset of the total LMXB population that have high inclinations ($i \sim 70$–90°) are the dipping and eclipsing sources (Díaz Trigo et al. 2006). Out of the 13 LMXB dipping sources (dippers from now) that host a neutron star, 6 systems show complete eclipses (D'Aì et al. 2014). These systems present a variety of spectro-temporal signatures that allow efficient means of probing the accretion disc, its atmosphere, and possible structures on it.

Absorbers responsible for producing the intensity dips are understood to be vertical structures present on the outer accretion disc, with asymmetric azimuthal distribution (White & Swank 1982; Boirin et al. 2005). Spectroscopic studies in a set of six dippers (EXO 0748-676, 4U 1254-690, 4U 1624-490, MXB 1659-298, 4U 1746-371, and 4U 1915-05) revealed that the spectral continuum during dips could be well described by simple ionized absorber models (Díaz Trigo et al. 2006).

High inclination systems have also been found to exhibit X-ray disc winds that are an important aspect in understanding the process of accretion/ejection, particularly in LMXBs (Miller et al. 2011, 2015; Ponti, Muñoz-Darias & Fender 2014). Disc-wind outflow signatures have been detected in the form of high-ionization Fe absorption lines with large outflow velocities in the soft spectral state (Neilsen & Lee 2009; Ponti et al. 2012). The fact that these absorption lines are seen only in high inclination sources indicate that these absorbers have an equatorial distribution. In both black hole and neutron star binaries, equatorial disc-wind outflow signatures have been detected only in their soft spectral state (Neilsen & Lee 2009; Miller et al. 2011; Ponti et al. 2012, 2014). Díaz Trigo et al. (2006) detected highly ionized Fe absorption lines (Fe XXV and Fe XXVI) in six high inclination dippers. Our current study focuses on one such high inclination LMXB, XTE J1710-281, with an aim to bring out important timing and spectral features in the source.

XTE J1710-281 is a transient eclipsing LMXB that was discovered in 1998 serendipitously, with *RXTE* (Markwardt et al. 1998). It is a highly inclined binary system viewed edge-on with an inclination angle i $\sim$75°–80° (Younes, Boirin & Sabra 2009). It shows

★ E-mail: graman@rri.res.in (GR); bpaul@rri.res.in (BP)

X-ray eclipses every 3.28 h with an average eclipse duration of ∼420 s (Jain & Paul 2011). This LMXB also exhibits X-ray intensity dips. The discovery of Type 1 thermonuclear bursts indicated that the compact object is a neutron star and the distance to the source was constrained using the Type-1 bursts to be between 15 and 20 kpc (Markwardt, Swank & Strohmayer 2001). The spectrum measured with RXTE PCA was consistent with a thermal bremsstrahlung ($kT = 14 \pm 3$ keV) or a power law (photon index 1.8 ± 0.1), with an absorption column density $N_{\rm H} < 2 \times 10^{22}$ cm^{-2} (Markwardt et al. 1998). Younes et al. (2009) reported spectral changes during dipping intervals using *XMM–Newton* observations in 2004 and compared the partial neutral absorber and ionized absorber models. Absorption lines due to ionized species like Fe XXV and Fe XXVI observed in other dippers (e.g. EXO 0748-676: Ponti et al. 2014; 4U 1323-62 and 4U 1624-490: Boirin et al. 2005) were not detected in their 2004 *XMM–Newton* observation.

XTE J1710-281 resembles a well-studied eclipsing source EXO 0748-676 in many ways. Both are high inclination LMXBs that show frequent thermonuclear X-ray bursts and intensity dips in their light curves. EXO 0748-676 has an orbital period of 3.82 h and displays pre-eclipse dips that vary significantly within short time-scales (Parmar et al. 1986; Raman & Paul 2017). Jain & Paul (2011) carried out extensive eclipse timing studies for XTE J1710-281 and reported two orbital period glitches which are similar to the period glitches observed in EXO 0748-676 (Wolff et al. 2009).

In this work, we have analysed archival data from *Chandra* and *Suzaku* for XTE J1710-281 to study the accretion disc dynamics in the context of the dip evolution and continuum spectral changes from persistent to dipping intervals. We then compare it with the eclipsing LMXBs, EXO 0748-676, and AX J1745.6-2901.

2 OBSERVATIONS AND DATA REDUCTION

We have analysed archival X-ray observations of XTE J1710-281 from *Chandra* and *Suzaku* observatories, a summary of which is presented in Table 1.

2.1 *Chandra*

XTE J1710-281 was observed with the *Chandra X-ray Observatory* (Weisskopf et al. 2002) on 2011 July 23 and August 7. The archival data for each Obs-ID (12468 and 12469) had an exposure of ∼75 ks with the ACIS-S detector using the High Energy Transmission Grating Spectrometer (Canizares et al. 2000). The data were processed using the CIAO software version 4.7. A level 2 data set was produced using the *chandra_repro* script. The ACIS light curve and spectra were extracted within a source region of 4 arcsec. The pile-ups for *Chandra* observations were computed using the web PIMMS version 4.8.[1] The ACIS-camera suffered from heavy photon pile-up (∼ 65 per cent) for the zeroth order and so the zeroth-order data are not used for further analysis of these two Obs-IDs. All the subsequent analysis are done with *Chandra* first-order HETG. The HETG first-order grating spectra, arf and rmf were produced during the level 2 processing using the *chandra_repro* script. The *combine_grating_spectra* tool was used to produce a co-added grating spectrum for the plus and minus first-order spectra of the HETG. The corresponding arf and rmf files were averaged. The spectra were rebinned to obtain a minimum of 50 counts per bin.

[1] http://cxc.harvard.edu/toolkit/pimms.jsp

2.2 *Suzaku*

The X-ray Imaging Spectrometer (XIS) aboard *Suzaku* covers the energy range of 0.2–12 keV (Koyama et al. 2007). The three operational XIS detectors: XIS0, XIS1, and XIS2 have been used for this current analysis. The *Suzaku* Obs-ID 404068010 had a useful exposure of ∼75 kilosec. The XIS detectors were operated in the standard data mode with normal window operation that provided a timing resolution of 8 s. The unfiltered event files were reprocessed with the CALDB version 20160607 and HEASOFT version 6.16. The XIS event files were checked for pile-up using the ftool 'pileest' and were found to be free from photon pile-up (less than 0.01 per cent). The reprocessed event files were used to extract light curves and spectra from a circular region of 240 arcsec around the source centroid. A circular region of the same size far away from the source centroid was selected for the background. Corresponding response file was generated by using the FTOOLS task *xisresp* using the CALDB mentioned above. In the case of *Suzaku* spectra, the spectra from the front-illuminated CCDs (XISs 0 and 3), and the back illuminated CCD (XIS-1) were fit simultaneously in the energy range of 0.6–9 keV keeping the instrument normalizations free. Due to artificial structures in the XIS spectra around the Si and Au edge, the energy range of 1.7–2.3 keV was neglected. The XIS spectra were rebinned to contain 100 counts per bin.

3 TIMING ANALYSIS

3.1 Light curve and average orbital profile

Since the ACIS zeroth-order light curve was heavily piled up, we extracted HETG first-order plus and minus arms light curves. Background-subtracted and energy-dependent (described in detail in Section 3.3) first-order light curves between 0.5 and 10 keV for *Chandra* Obs-IDs 12468 and 12469 were extracted with a bin size of 1.74 s and are plotted with a 200 s binning (the top left and right panels of Fig. 1). The light curves display more than six orbital cycles with sharp X-ray eclipses. X-ray intensity dips are seen to occur at orbital phases prior to the eclipse. The depth and width of the dips are seen to vary from one orbital cycle to the next, as described in detail in the next subsection. The first-order light curves from both the *Chandra* observations also exhibit 7 and 5 type-1 bursts, respectively, as mentioned in Table 1.

We also extracted light curve for the *Suzaku* observation in the 0.5–10 keV energy band with a time bin size of 8 s and plotted it with a bin size of 100 s (the bottom panel of Fig. 1). The light curve contains large data gaps, with incomplete sampling of persistent, dipping, and eclipsing intervals. The light curve shows a total of six thermonuclear X-ray bursts during this observation.

In order to compare the average orbital profile, specially the dip features between the different observations, we folded the light curves with the orbital period of 11812.66 s (Jain & Paul 2011), at a reference epoch of MJD 55278.29, 55762.79 and 55766.895 for the *Suzaku* observation and *Chandra* Obs-IDs 12468 and 12469, respectively. In order to exclude the thermonuclear bursts, time filters were applied to the light curves. These time windows were ∼100 s in duration. The average orbital profile is shown in Fig. 2 with dips covering the phase range of 0.6–0.9. The *Chandra* Obs-IDs 12468, 12469, and *Suzaku* light curves show slightly different folded orbital profile features. The duty cycle of a dip is defined as the duration of the dip as a fraction of the total orbital period. The pre-eclipse dips for the *Chandra* Obs-ID 12468 and *Suzaku* have duty cycle of nearly 40 per cent,

Table 1. Table detailing the different observations used in the current analysis.

Observatory	Obs-ID	Instrument	Date of observation (MJD)	Exposure (ks)	Number of type-1 X-ray bursts
Chandra	12468	HETG	23-07-2011 (55765)	75.1	7
Chandra	12469	HETG	07-08-2011 (55780)	75.1	5
Suzaku	404068010	XIS	23-03-2010 (55278)	76.1	6

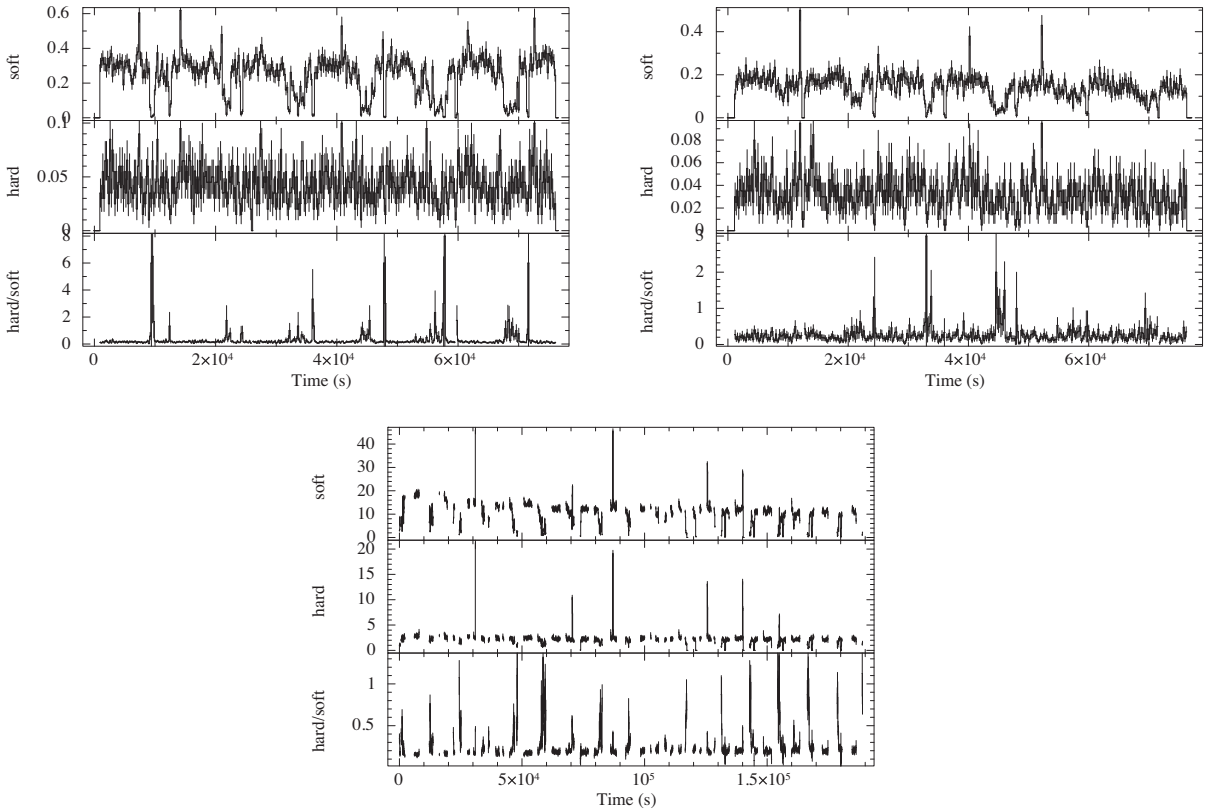

Figure 1. Light curves from the first-order HETG *Chandra* Obs-ID 12468 (top-left), 12469 (top-right) with a bin size of 200 s and *Suzaku* (bottom) with a bin size of 100 s are shown. The light curves, extracted in two energy bands soft (0.5–5 keV) and hard (5–10 keV), are shown along with the hardness ratio in the bottom panel for all the three Obs-IDs. An increase in the hardness ratio is observed during dipping. Type-1 thermonuclear X-ray bursts are also observed in all the light curves.

while for the *Chandra* Obs-ID 12469, it is nearly 30 per cent. Along with the pre-eclipse dips, the *Suzaku* profile shows a bump at around phase 0.3, while the *Chandra* Obs-IDs 12468 and 12469 profiles show a less intense secondary dip at phase ∼0.4 (duty cycle 10 per cent).

3.2 Orbit to orbit evolution of dips

While examining the *Chandra* data, an orbit-to-orbit evolution of dips is seen for the first time in the source (Fig. 3). The evolution of the depth and width in each subsequent orbit is clearly visible for both the observations. The pre-eclipse dip is observed to be with and without sub-structures in different orbital cycles. An earlier study of the dips made by Younes et al. (2009) in 2004 using *XMM–Newton* also reported presence of narrow absorption dips in one single orbital cycle alone. For both the observations, the duty cycle of the dips range from about 10 per cent to nearly 50 per cent, possibly indicating variable absorber azimuthal distribution above the disc plane. The depth of the dips vary between 20 and 90 per cent, signifying variable absorber column density along our line-of-sight between successive orbital cycles. Unlike the light curves from the *Chandra* observations, the *Suzaku* light curve has data gaps. We cannot therefore investigate the dips in the light curve in successive orbits.

3.3 Energy dependence of dips

To investigate the energy dependence of the dips, we extracted background subtracted light curves in two energy bands: 0.5–5 and 5–10 keV for all the observations. Fig. 1 shows the energy-dependent intensity variations in the light curves for the three observations. The soft X-ray light curve shows more prominent dips as compared to the hard-X-ray band. As a result, the hardness ratio increases during the X-ray dips, with the deeper troughs showing an increased hardness ratio compared to the shallower one. Although the *Suzaku* observation has periodic large data gaps, a periodic increase in the hardness ratio with interval same as the orbital period indicate it to be due to the dips in the same orbital phase range as the *Chandra*

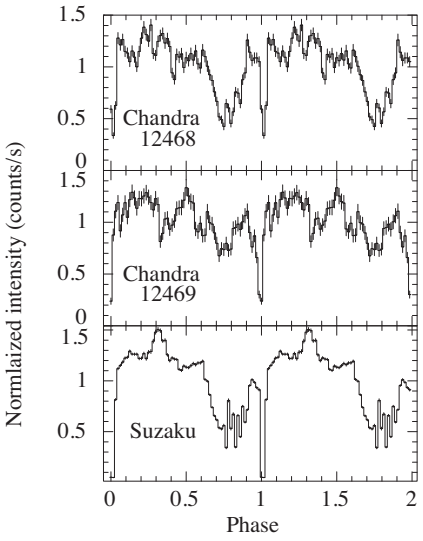

Figure 2. The average orbital profile of the two *Chandra* observations 12468 (top) and 12469 (middle) folded at 11812.66 s. The bottom panel shows the average *Suzaku*-folded pulse profile. All three observations display a clear dip at the orbital phase just before the eclipse.

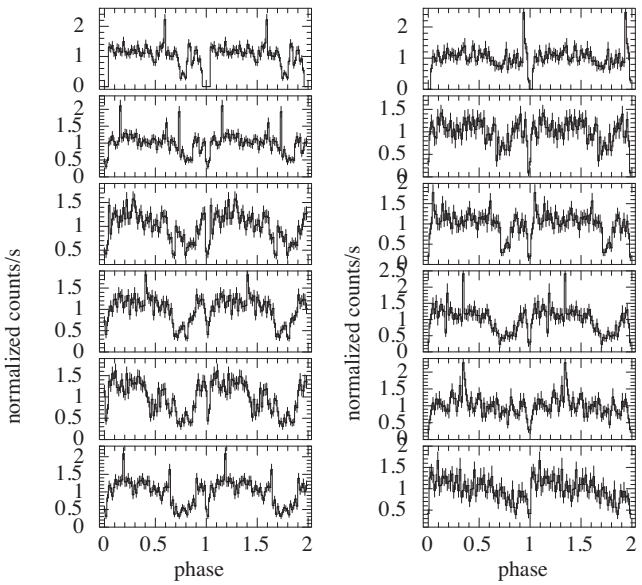

Figure 3. The orbit-to-orbit intensity modulations are shown for the *Chandra* Obs-IDs 12468 (left) and 12469 (right) first-order light curve. A clear evolution of the dip parameters (depth, width, and shape) as a function of time is observed.

light curves. The increase in hardness ratio during dipping intervals has been observed before by Younes et al. (2009) using *XMM–Newton* observations for this source and for other dipping sources like 4U 1254-690, 4U 1323-62, 4U 2127+11, etc. (Ioannou et al. 2002; Boirin et al. 2005; Díaz Trigo et al. 2009).

4 SPECTRAL ANALYSIS

4.1 Time-averaged spectroscopy

We performed spectroscopy of XTE 1710-281 averaged over the entire stretch of the observations for the *Chandra* and *Suzaku* data. Spectral fitting was performed using XSPEC (Arnaud 1996) version 12.8.1. The photoelectric cross-sections of Wilms, Allen & McCray (2000) have been used to model the line-of-sight absorption by neutral gas with solar abundances (the '*TBabs*' XSPEC model). The cross-section for X-ray absorption by the ISM is computed as the sum of the cross-sections for X-ray absorption due to the gas-phase ISM, the grain-phase ISM, and the molecules in the ISM.

At first all the spectra were fitted with a power law with a single absorption component accounting for the foreground absorption which includes the line-of-sight interstellar absorption as well as absorption local to the source. Fitting a simple power-law model to the *Chandra* observation 12468 resulted in a reduced chi-squared value of ∼0.65. We therefore re-binned the spectrum to at least 1 count per bin and applied C-statistic which is appropriate for the quality of the data. The spectral fit with an absorbed power-law provided an acceptable fit with a C-stat/d.o.f. of 2305/3841 (the top left-hand panel of Fig. 4).

In the case of the other *Chandra* (Obs-ID 12469) and *Suzaku* observation, the fit with a simple absorbed power law proved to be unsatisfactory with large systematic residuals particularly in the energy range of 1.2–2.0 keV. To account for this, we added another absorption component in the form of a partial covering absorber. This can be explained due to absorption by local structures in the accretion disc (causing the pre-eclipse dips). We tried to fit the spectra with both a partial covering neutral absorber (XSPEC model '*pcfabs*') and partial covering ionized absorber (XSPEC model '*zxipcf*', Reeves et al. 2008). For the *Chandra* Obs-ID 12469, the addition of partial covering neutral absorber improved the χ^2 by 12.1 (Δd.o.f. of 2) and the addition of partial covering partially ionized absorber improved the χ^2 by 79.5 (Δd.o.f. of 3).

In the case of the *Suzaku* observation, the reduction in χ^2 obtained by adding the partial covering neutral and ionized absorber models was 37 (Δd.o.f. of 2) and 50 (Δd.o.f. of 3), respectively. The fit with the ionized absorber model proved to be better both in terms of absence of systematic structures in the residuals and a lower value of reduced χ^2. A power-law model with a partially ionized partial covering absorber model was therefore chosen as the best-fitting model and all subsequent analysis were performed with this.

In addition to the modelling of the continuum, we detected several absorption lines and edge features in the *Chandra* and *Suzaku* spectra. In the time-averaged *Suzaku* spectrum, a broad emission feature is observed at ∼0.72 keV with an equivalent width 93.03 ± 66.98 eV. This is probably a complex due to unresolved Fe L shell lines. Two additional weak absorption lines are observed at 6.60 ± 0.03 and 7.01 ± 0.03 keV. These two absorption lines were modelled using Gaussian absorption model. The addition of the 0.72 keV feature improved the χ^2 by 31, with the addition of three new parameters for a Δd.o.f of 3. Further addition of the two absorption features at 6.6 and 7.01 keV progressively improved the χ^2 by 23 (Δd.o.f of 3) and 7 (Δd.o.f of 3), respectively. The 6.6 keV line is detected with an equivalent width of 4.28 ± 0.47 eV. The 7.01 keV absorption line, being not statistically significant is detected with an equivalent width of only ∼0.58 ± 0.49 eV. The best fits for the time-averaged spectra after adding all the components gives a reduced χ^2 of 1.10 for 566 d.o.f. for the *Chandra* Obs-ID 12469 spectrum and 0.95 for 599 d.o.f for the *Suzaku* spectrum.

Although we do not detect the ∼6.6 keV feature in the *Chandra* HETG spectrum, we cannot rule out their presence in the corresponding spectra. This is because, for the count rate of XTE J1710-281, these lines would be below the detection threshold of HETG considering its lower effective area w.r.t the XIS. In order to examine if such a feature would be detectable in the *Chandra* spectrum,

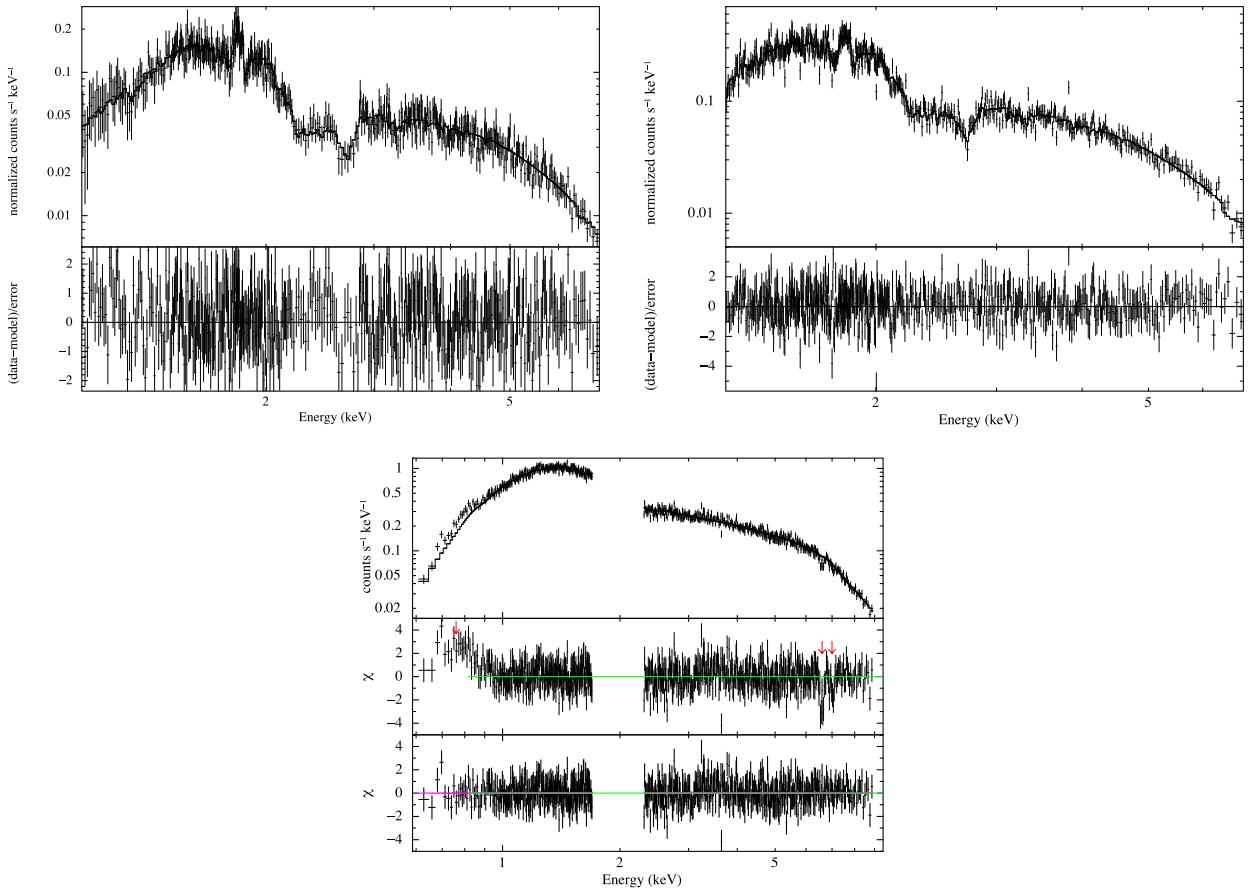

Figure 4. The time-averaged best-fitting spectra for *Chandra* Obs-IDs 12468 (top-left), 12469 (top-right), and *Suzaku* (bottom) are shown. For the *Chandra* Obs-ID 12468 spectrum, the plot has been re-binned for visual clarity. In the *Suzaku* spectrum, the residuals are indicated without (top residual panel) and with (bottom residual panel) the 0.72, 6.59, and 7.01 keV lines modelled.

a Gaussian absorption feature (the 'gabs' model in XSPEC) was introduced at 6.60 keV, with the line energy and width fixed to the parameter values obtained in the Suzaku spectra. This model is, however, not statistically preferred ($\Delta\chi^2$ of 0.11 for Δd.o.f of 3) as an additional component over the continuum. We therefore do not include it in the spectral fit.

Table 2 shows the best-fitting parameters along with the fluxes measured for the *Chandra* and *Suzaku* observations. Fig. 4 shows the best-fitting average HETG first-order spectra for *Chandra* Obs-ID 12469 and the XIS0 *Suzaku* spectra. The derived absorbed fluxes (0.5–8 keV) for the *Chandra* (Obs-IDs 12468 and 12469) and the *Suzaku* observations in order are $5.14 \pm 0.20 \times 10^{-11}$, $7.94 \pm 0.10 \times 10^{-11}$, and $4.10 \pm 0.07 \times 10^{-11}$ erg cm^{-2} s^{-1}, respectively. The *Chandra* Obs-ID 12469 shows a steeper power-law index and larger flux compared to the *Chandra* Obs-ID 12468 and *Suzaku* observations.

4.2 Intensity-resolved spectroscopy

In order to probe the changes in the spectrum from the persistent and dipping intervals, we carried out an intensity resolved spectral analysis of the *Chandra* and *Suzaku* observations. In order to perform this exercise, we first excluded the intervals corresponding to thermonuclear bursts and eclipses. We then defined persistent and dipping intervals based on the count rate from the light curves of the corresponding observations. For the *Chandra* observations, the persistent emission is seen to have an average count rate of 0.25 counts s^{-1} (Fig. 1). Time intervals that had intensities below 75 per cent of the average persistent count rate were considered as dipping intervals. We then extracted spectra corresponding to those intervals. The *Chandra* intensity resolved spectra were grouped to contain 50 counts per energy bin. We did not carry out intensity resolved spectral analysis for the *Chandra* Obs-ID 12468 due to statistical limitations.

Since the *Suzaku* light curve contained incompletely sampled dips, it was not possible to identify dipping time intervals from the light curve. Therefore, a count rate cut of 75 per cent of the average persistent count rate (about 2 counts s^{-1}), similar to what was used for the *Chandra* analysis, was adopted to identify the dipping intervals. The corresponding spectra for the persistent and dipping intervals were extracted. A different grouping scheme was adopted for the persistent (minimum of 120 counts per bin) and dipping (minimum of 100 counts per bin) intervals, as compared to the time-averaged *Suzaku* spectrum to have comparable statistics. The same background and response files that were used to fit the persistent spectra were taken for the fits.

We consider the cause of the dipping activity to be absorption due to the passage of the vertical structures obscuring our view to the source (White & Swank 1982; Díaz Trigo et al. 2006). In this case, we may assume that the underlying continuum spectrum does not change during the duration of the observation, and the spectral changes during the dipping intervals are solely due to the

Table 2. Best-fitting spectral parameters for time-averaged *Chandra* (Obs-IDs 12468 and 12469) HETG spectra and *Suzaku* XIS0 spectra. The errors are quoted at 90 per cent confidence interval.

Model parameter	Model	*Chandra* Obs-ID 12468	*Chandra* Obs-ID 12469	*Suzaku*
nH^{fore} ($10^{22}cm^{-2}$)	**TBabs**	0.21 ± 0.1	0.72 ± 0.1	0.51 ± 0.03
nH ($10^{22}cm^{-2}$)	**zxipcf**		$45.3^{-10.4}_{+9.2}$	45.96 ± 10.1
log(ξ)	**zxipcf**		3.03 ± 0.1	1.91 ± 0.34
Cov. f	**zxipcf**		0.56 ± 0.1	0.45 ± 0.05
Power-law index	**po**	1.54 ± 0.2	2.45 ± 0.1	1.98 ± 0.06
E_{gabs} (keV)	**gabs**			6.60 ± 0.03
EW (eV)	**gabs**			4.28 ± 0.47
E_{gabs} (keV)	**gabs**			7.01 ± 0.03
EW (eV)	**gabs**			0.58 ± 0.49
E_{gaus} (keV)	**gaus**			0.72 ± 0.01
EW (eV)	**gaus**			93.03 ± 66.98
red. χ^2		C-stat/d.o.f.: 2305/3841	1.10 for 566 d.o.f.	0.95 for 599 d.o.f
Flux (erg cm^{-2} s^{-1})[a]		$5.14 \pm 0.20 \times 10^{-11}$	$7.94 \pm 0.10 \times 10^{-11}$	$4.10 \pm 0.07 \times 10^{-11}$

Note: [a]Flux is measured from 0.5 to 8 keV. ξ is in erg cm s^{-1}.

passage of this absorbing material along our line of sight. In order to demonstrate this, we fit the persistent and the dipping spectra simultaneously linking the parameters of the continuum emission, i.e. the power-law component. The absorption components are left free. The persistent emission is not used for constraining the ionized absorber properties. We fix the energy and width of the emission and absorption lines and edges in the *Chandra* and *Suzaku* spectra to the corresponding values obtained in the average spectra.

In the case of the intensity resolved spectral fit for the *Chandra* Obs-ID 12469, the line-of-sight neutral hydrogen column density was fixed to the time-average value. This was because the errors obtained on this parameter, if left free for each component, was very large. The *Chandra* intensity resolved spectrum showed a residual, resembling an edge around 2.8 ± 0.2 keV, which we have modelled using an edge model. This edge, possibly indicating the presence of S XVI, removes the residual and improves the fit ($\Delta\chi^2$ of 356.49 and Δd.o.f. of 3). The addition of this component in the time average spectrum only shows a small improvement in χ^2 ($\Delta\chi^2$ of 5), making it a weak detection. We observe an increase in the column density of the ionized absorber and a decrease in the ionization state from the persistent to dipping spectra. A similar change in the ionized absorber parameters is observed for the intensity resolved *Suzaku* spectra as well. The column density of the ionized absorber increases from $0.36 \pm 0.15 \times 10^{22}$ to $14.9 \pm 1.8 \times 10^{22}$ cm^{-2} and the ionization parameter log(ξ), shows a decrease from 2.6 ± 0.2 to 1.45 ± 0.1 (where ξ is in erg cm s^{-1}) as we go from the persistent to the dipping spectra. We fixed the 6.60 and 7.01 keV absorption line parameters, and the 0.72 keV broad emission-line parameters to the time-averaged spectral parameter values. The best-fitting spectra for the intensity resolved *Chandra* and *Suzaku* observations are shown in Fig. 5, and Table 3 shows the best-fitting spectral parameters.

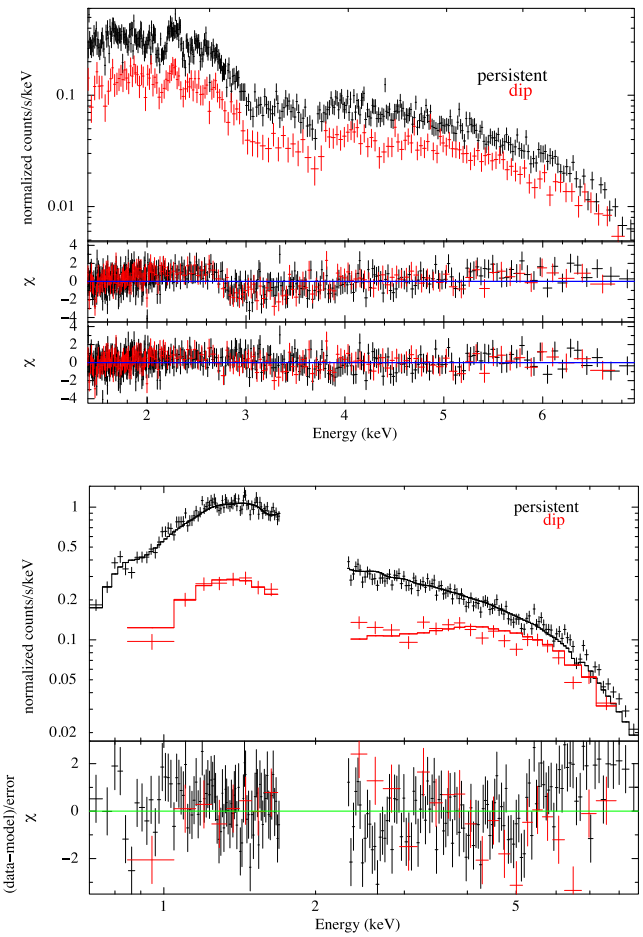

Figure 5. Intensity resolved spectra for the persistent and dip epochs are fit simultaneously for *Chandra* Obs-ID 12469 (top) and *Suzaku* (bottom) observations. The two panels showing the residuals in the *Chandra* spectra correspond to the edge at 2.8 keV left unmodelled (top residual plot) and modelled (bottom residual plot). The best-fitting spectrum for only the XIS0 is shown for the *Suzaku* observation.

5 DISCUSSION

We have carried out spectro-temporal analysis of the dipping LMXB XTE J1710-281 using archival *Chandra* and *Suzaku* observations. We have observed evolution in the dip strength, duration, and shape between successive orbital cycles, indicating evolution of the accretion disc structures in the time-scale of hours. We have also detected highly ionized Fe species in the *Suzaku* spectra, which indicate signature of disc winds as observed in other dippers. The dip spectrum in *Chandra* and *Suzaku* observations is found to be best described by a power-law component with a spectral index of $\Gamma \sim 2$ with partial covering by a partially ionized absorber.

Table 3. Best-fitting spectral parameters for intensity resolved *Chandra* (Obs-ID 12469) HETG spectra and *Suzaku* XIS0 spectra. The errors are quoted at 90 per cent confidence interval.

Parameter	Model	*Chandra* Obs-ID 12469		*Suzaku*	
		Persistent	Dip	Persistent	Dip
nH^{fore} (10^{22} cm^{-2})	**TBabs**	0.72[a] (fixed)		0.23 ± 0.01	0.17 ± 0.06
nH (10^{22} cm^{-2})	**zxipcf**	$12.9^{-9.1}_{+17.2}$	65.6 ± 25.2	0.36 ± 0.15	14.9 ± 1.8
log(ξ)	**zxipcf**	$3.43^{-0.1}_{+0.57}$	$1.85^{+0.2}_{-1.0}$	2.6 ± 0.15	1.45 ± 0.1
Cov. f	**zxipcf**	0.65 ± 0.4	0.5 ± 0.02	0.67 ± 0.3	0.89 ± 0.01
Power-law index	**po**	2.57 ± 0.04		1.79 ± 0.02	
E (keV)	**edge**	2.8±0.2			
Max Tau	**edge**	0.45 ± 0.10			
red. χ^2		0.92 for 581 d.o.f.		1.13 for 375 d.o.f	

Note: [a]Frozen to the time-averaged spectral parameter value. ξ is in erg cm s^{-1}.

5.1 Evolution of the dips

High inclination LMXB sources exhibit intensity dips, which are usually characterized by increased spectral hardness (Díaz Trigo et al. 2009). These dips have been observed in some total eclipsing sources like EXO 0748-676, XTE J1710-281, and also in some partial eclipsing sources like 4U 2129+12 (Chou 2014). Recently, Galloway et al. (2016) discovered, in the LMXB source Aql X-1, intermittent episodes of dipping, similar to those observed in high inclination binaries. Detailed characterization of dip parameters like the dip orbital phase, width, and strength have been performed for many dippers to extract information of orbital period and also dynamics of the accretion disc structures (Chou 2014; Chou & Grindlay 2001; Hu, Chou & Chung 2008). Since dips are caused by absorption in the accretion disc structure, they are not exactly phase-locked, but they show phase jitters (e.g. ± 0.05 cycle for 4U 1915-05; Chou & Grindlay 2001). In the case of XTE J1710-281 (Younes et al. 2009 and the current work), on average, the dips are observed pre-dominantly at pre-eclipse orbital phases between the orbital phase range of 0.6–0.9. In the system EXO 0748-676, dips have also been seen at other orbital phases, even just after the eclipse (Raman & Paul 2017). A very interesting outcome of the current study of dips using *Chandra* observations is the evolving morphology from one orbital cycle to the next. The dip depth, width as well as shape (in terms of the number of narrow features present) are observed to vary. Irradiation-induced vertical structures (de Jong, van Paradijs & Augusteijn 1996; Pringle 1996) present usually at the outer accretion disc are azimuthally distributed in an asymmetric manner (Hakala et al. 2005). They are responsible for preferentially absorbing the primary X-ray photons at certain orbital epochs as was also observed in EXO 0748-676 (Parmar et al. 1986). The orbit-to-orbit dip profiles as seen in the *Chandra* light curves have different features, some are broad, some deep, and some even have narrow features, similar to what was observed by Younes et al. (2009) in the *XMM–Newton* light curve. Nevertheless, the presence of varying dip intensities in successive orbital cycles in *Chandra* indicates not just any structure, but an *evolving* one. Warped discs also present a very physically compelling solution to explain different X-ray modulations in LMXBs (Ogilvie & Dubus 2001). These warps can develop at various disc-radii and can modulate the X-ray emission at certain orbital epochs. Another possible explanation for a hour-time-scale-varying dip morphology could be the variable mass accretion splashes at the stream-impact point on the outer accretion disc (White & Swank 1982). At these locations, the disc-extent increases vertically leading to temporary structures that block the primary X-ray photons from reaching the observer.

5.2 Detection of ionized species of Fe

The broad 0.72 keV emission line detected in the *Suzaku* spectrum can be identified with an Fe L blend. It has an equivalent width of 93.03 ± 66.98 eV. Owing to the fact that XTE J1710-281 is a relatively faint source, the *Chandra* spectrum does not have enough photons below 1 keV and was therefore not able to detect a line of similar strength. Line emission in the spectral energy range of 0.7–2.0 keV, associated with the Fe L-shell ions, is understood to be a dominant spectral component arising in coronal plasmas (Liedahl, Osterheld & Goldstein 1995). Only ionized Fe ions (Fe XII and beyond) produce Fe L transitions that fall in the energy range of 0.7–2 keV. In addition, two narrow, weak absorption lines are observed at 6.60 and 7.01 keV in the *Suzaku* spectrum (see Table 2). The absorption line at ∼6.6 ± 0.03 keV is most likely a blend of Fe XIX to Fe XXV lines (Díaz Trigo et al. 2006; Ponti et al. 2014). Associating it to the nearest Fe XX–XXII transition at ∼6.58 keV (Jiménez-Bailón et al. 2007) results in a blue-shifted velocity of 789 km s^{-1} (see e.g. as computed in King et al. 2014). Such blue-shifted velocities correspond to outflows such as disc wind as observed in several other disc accreting high inclination sources. The 7.01 ± 0.03 keV is, however, only marginally detected and we do not compute the velocities for this line. Such features at ∼6.6 keV have been observed in other NS LMXBs, e.g. XB 1323-619 and XB 1916-053 (Boirin et al. 2005; Díaz Trigo et al. 2006). In their 2004 *XMM–Newton* observation of XTE J1710-281, Younes et al. (2009) did not detect absorption lines due to ionized species like Fe XXIV, Fe XXV, or Fe XXVI that are commonly observed in other dippers (e.g. EXO 0748-676: Ponti et al. 2014; 4U 1323-62 and 4U 1624-490: Boirin et al. 2005). However, they have derived upper limits on the equivalent width of the 6.65 keV absorption line corresponding to the Fe XXV 1s–2p transition as 114, 50, and 73 eV in the persistent, shallow-dipping, and deep-dipping spectra, respectively.

We conservatively identify the edge feature at ∼2.8 keV in the *Chandra* spectra (within errors) as highly ionzed Sulphur species, S XVI, which has been observed in MR 2251-178 (Gofford et al. 2011), EXO 0748-676 (Ponti et al. 2014), GRS 1915+105 (Ueda, Yamaoka & Remillard 2009), and also in Cyg X-1 (Feng, Tennant & Zhang 2003). It is likely that, as seen in EXO 0748-676, the highly ionized absorber on the accretion disc could be responsible for the S XVI absorption edge as well.

Such high-ionization Fe lines are tracers for equatorial disc winds (Ponti et al. 2014). The lines are suspected to be produced by absorption due to photoionized gas (Ponti et al. 2015). The Fe XXV K α ($E = 6.697$ keV) and Fe XXVI K α ($E = 6.966$ keV), as well as Fe XXV K β ($E = 7.880$ keV) absorption lines have been observed in three other eclipsing sources AX J1745.6-2901 (Hyodo et al. 2009), EXO 0748-676 (Ponti et al. 2014), and IGR J17451-3022 (Bozzo et al. 2016). Hyodo et al. (2009) suggested a disc-corona origin for these lines in the source AX J1745.6-2901, since they were observed at all orbital phases. Other non-eclipsing, high-inclination dippers like 4U 1254-690, 4U 1624-490, and MXB 1659-298 also show these features, suggesting an equatorial origin for these photoionized absorbing gas (Ponti et al. 2014). In black hole binaries, these absorption features were found to have high outflow velocities and therefore were assumed to be equatorial winds (see Ponti et al. 2012, 2014).

In a recent review, Díaz Trigo & Boirin (2016) show that from a total of 18 LMXBs exhibiting presence of photoionized plasma in the form of absorption lines of Fe XXV and Fe XXVI, 16 systems have highly ionized plasma ($\log(\xi) > 3$). However, there are four systems that exhibit *both* high ($\log(\xi) > 3$) and low ($\log(\xi) < 3$) photoionization and two systems (MAXI J1305-704 and GX 339-4) that show only low photoionization. Results obtained from the *Suzaku* observation in this work indicate that XTE J1710-281 could be one such system whose photoionized plasma has low ionization. Such photoionized plasma can be irradiation induced, or even be the result of thermal or magnetic instabilities, etc.

5.3 Nature of the absorber

Various models have been proposed to explain the continuum emission in dippers. In order to particularly describe the Comptonized component, a number of single and multicomponent continuum power-law models have been previously explored. One set of models (Boirin et al. 2005; Díaz Trigo et al. 2006) incorporate a neutral or ionized absorber partially or completely covering the power law as well as the blackbody emission during dips. These models explain the dip spectra in sources like 4U 1323-62, EXO 0748-676, and 4U 1254-690. Another set of models (Parmar et al. 1985; Bonnet-Bidaud et al. 2001; Oosterbroek et al. 2001; Younes et al. 2009) incorporate two components. In these models, one fraction of the power-law component is partially covered by an ionized or a neutral absorber and the remaining fraction is left uncovered. These models have been invoked to describe the dipping spectra in EXO 0748-676. Finally, the third set of models are the complex-continuum models (Church et al. 1998; Bałucińska-Church et al. 1999). These models require two independent absorbing components: one for the extended Comptonized power-law emission and another for the point-like blackbody emission. Again, these complex models allow for neutral as well as ionized absorbers for the Comptonized continuum component. Dippers like 4U 1323-62 were modelled in this manner (Boirin et al. 2005).

In the case of XTE J1710-281, the spectral properties of the dips are well described by an ionized absorber that partially obscures the non-thermal emission and does not require us to invoke other complicated models.

Considering that the ionized absorber is located at the outer accretion disc, we can compute the ratio of thickness d, of a slab of the absorber, with respect to the distance r, between the ionizing source and the absorber. For this, we consider the circularization radius to be the minimum possible value for the accretion disc radius r and compute it using equation 4.21 of Frank, King & Raine (1992) for a system with mass ratio $q \sim 0.3$. We obtain $R_{\rm circ} \sim 0.32 R_{\odot}$. Since $\xi = L/n_e r^2$, and $n_e \sim {n_H}^{zxipcf}/\mathrm{d}$, we compute the ratio,

$$d/r = \frac{r \times \xi \times {n_H}^{zxipcf}}{L},$$

where ξ is the ionization parameter, L is the source luminosity, $n_{\rm e}$ is the electron number density, and ${n_H}^{zxipcf}$ is the ionized absorber column density. Assuming a distance of 15 kpc to the source (Markwardt et al. 2001) and a considering a flux of 7.9×10^{-11} erg cm^{-2} s^{-1} (Table 2), we obtain a source luminosity of 2×10^{36} erg s^{-1}. This gives us d/r ratios of 0.03 and 0.007 for the persistent and dipping intervals, respectively.

Also, there is strong reason to believe that the absorber responsible for the X-ray intensity dips also causes the Fe line absorptions as well, mainly because these lines are observed only in high inclination dipping sources. The relative line strengths in these different intensity epochs (persistent and dipping) can allow us to probe the absorber characteristics. For example, lines detected during the dips correspond to electronic transitions from less ionized species than during the persistent (Younes et al. 2009). However, we were unable to compare the line parameters in detail because of the weak line depths and statistical limitations of the data set.

6 CONCLUSIONS

We have studied the eclipsing NS X-ray binary XTE J1710-281 using archival *Chandra* and *Suzaku* observations. Using *Chandra* folded orbital profiles, we detected an evolution of the dip morphology from orbit to orbit, indicating accretion disc structures, which seem to evolve in time-scales as short as a few hours. The intensity resolved *Chandra* and *Suzaku* continuum spectra are best described using a power law that is partially absorbed by ionized material. We have detected signatures of accretion disc winds in the *Suzaku* spectra, in the form of highly ionized Fe absorption lines at ~6.60 and ~7.01 keV and a broad Fe emission line complex at 0.72 keV. In the *Chandra* spectra, we detect the presence of an absorption edge at 2.8 ± 0.2 keV, corresponding to the highly ionized S XVI species. Fe lines are detected only in *Suzaku* spectrum, but we cannot rule out their presence in the *Chandra* (as we mention) and *XMM–Newton* (as Younes et al. 2009 mention) observations. There is no clear correlation between the flux, shape of the continuum, and presence/absence of lines in these observations. The shape of the continuum is consistent between the different observations: for the case of the *XMM–Newton* observation (Younes et al. 2009) and also for the case of *Chandra* and *Suzaku* observations (present work). Future observations of this object will help us to understand the distribution of ionized matter on the accretion disc and disc structure evolution scenarios better.

ACKNOWLEDGEMENTS

This work has made use of data obtained from the High Energy Astrophysics Science Archive Research Center (HEASARC), provided by the NASA Goddard Space Flight Center. We thank the referee for constructive comments and suggestions.

REFERENCES

Arnaud K. A., 1996, in Jacoby G. H., Barnes J., eds, ASP Conf. Ser. Vol. 101, Astronomical Data Analysis Software and Systems V. Astron. Soc. Pac., San Francisco, p. 17

Bałucińska-Church M., Church M. J., Oosterbroek T., Segreto A., Morley R., Parmar A. N., 1999, A&A, 349, 495

Boirin L., Méndez M., Díaz Trigo M., Parmar A. N., Kaastra J. S., 2005, A&A, 436, 195
Bonnet-Bidaud J. M., Haberl F., Ferrando P., Bennie P. J., Kendziorra E., 2001, A&A, 365, L282
Bozzo E. et al., 2016, A&A, 589, A42
Canizares C. R. et al., 2000, ApJ, 539, L41
Chou Y., 2014, Res. Astron. Astrophys., 14, 1367
Chou Y., Grindlay J. E., 2001, ApJ, 563, 934
Church M. J., Bałucińska-Church M., Dotani T., Asai K., 1998, ApJ, 504, 516
D'Aì A., Iaria R., Di Salvo T., Riggio A., Burderi L., Robba N. R., 2014, A&A, 564, A62
de Jong J. A., van Paradijs J., Augusteijn T., 1996, A&A, 314, 484
Díaz Trigo M., Boirin L., 2016, Astron. Nachr., 337, 368
Díaz Trigo M., Parmar A. N., Boirin L., Méndez M., Kaastra J. S., 2006, A&A, 445, 179
Díaz Trigo M., Parmar A. N., Boirin L., Motch C., Talavera A., Balman S., 2009, A&A, 493, 145
Feng Y. X., Tennant A. F., Zhang S. N., 2003, ApJ, 597, 1017
Frank J., King A., Raine D., 1992, Accretion Power in Astrophysics, Cambridge University Press, Cambridge
Galloway D. K., Ajamyan A. N., Upjohn J., Stuart M., 2016, MNRAS, 461, 3847
Gofford J. et al., 2011, MNRAS, 414, 3307
Hakala P., Ramsay G., Muhli P., Charles P., Hannikainen D., Mukai K., Vilhu O., 2005, MNRAS, 356, 1133
Hu C.-P., Chou Y., Chung Y.-Y., 2008, ApJ, 680, 1405
Hyodo Y., Ueda Y., Yuasa T., Maeda Y., Makishima K., Koyama K., 2009, PASJ, 61, S99
Ioannou Z., Naylor T., Smale A. P., Charles P. A., Mukai K., 2002, A&A, 382, 130
Jain C., Paul B., 2011, MNRAS, 413, 2
Jiménez-Bailón E., Santos-Lleó M., Piconcelli E., Matt G., Guainazzi M., Rodríguez-Pascual P., 2007, A&A, 461, 917
King A. L. et al., 2014, ApJ, 784, L2
Koyama K. et al., 2007, PASJ, 59, 245
Lewin W. H. G., Clark G. W., 1980, in Ehlers J., Perry J. J., Walker M., eds, Ann. New York Acad. Sci., Vol. 336, Ninth Texas Symp. Relativ. Astrophys., New York Academy of Sciences, New York, p. 451
Liedahl D. A., Osterheld A. L., Goldstein W. H., 1995, ApJ, 438, L115
Markwardt C. B., Marshall F. E., Swank J., Takeshima T., 1998, IAU Circ., 6998
Markwardt C. B., Swank J. H., Strohmayer T. E., 2001, in Bull. Am. Astron. Soc., Vol. 33, American Astronomical Society Meeting Abstracts, p. 1350
Miller J. M., Maitra D., Cackett E. M., Bhattacharyya S., Strohmayer T. E., 2011, ApJ, 731, L7
Miller J. M., Fabian A. C., Kaastra J., Kallman T., King A. L., Proga D., Raymond J., Reynolds C. S., 2015, ApJ, 814, 87
Neilsen J., Lee J. C., 2009, Nature, 458, 481
Ogilvie G. I., Dubus G., 2001, MNRAS, 320, 485
Oosterbroek T., Parmar A. N., Sidoli L., in't Zand J. J. M., Heise J., 2001, A&A, 376, 532
Parmar A. N., Gottwald M., Haberl F., Giommi P., White N. E., 1985, in Burke W. R., ed., ESA SP-236, Recent Results on Cataclysmic Variables. The Importance of IUE and Exosat Results on Cataclysmic Variables and Low-Mass X-Ray Binaries
Parmar A. N., White N. E., Giommi P., Gottwald M., 1986, ApJ, 308, 199
Ponti G., Fender R. P., Begelman M. C., Dunn R. J. H., Neilsen J., Coriat M., 2012, MNRAS, 422, 11
Ponti G., Muñoz-Darias T., Fender R. P., 2014, MNRAS, 444, 1829
Ponti G. et al., 2015, MNRAS, 446, 1536
Pringle J. E., 1996, MNRAS, 281, 357
Raman G., Paul B., 2017, New Astron., 54, 122
Reeves J., Done C., Pounds K., Terashima Y., Hayashida K., Anabuki N., Uchino M., Turner M., 2008, MNRAS, 385, L108
Ueda Y., Yamaoka K., Remillard R., 2009, ApJ, 695, 888
Weisskopf M. C., Brinkman B., Canizares C., Garmire G., Murray S., Van Speybroeck L. P., 2002, PASP, 114, 1
White N. E., Swank J. H., 1982, ApJ, 253, L61
Wilms J., Allen A., McCray R., 2000, ApJ, 542, 914
Wolff M. T., Ray P. S., Wood K. S., Hertz P. L., 2009, ApJS, 183, 156
Younes G., Boirin L., Sabra B., 2009, A&A, 502, 905

This paper has been typeset from a TEX/LATEX file prepared by the author.